

TDCOSMO

VI. Distance measurements in time-delay cosmography under the mass-sheet transformation

Geoff C.-F. Chen¹, Christopher D. Fassnacht¹, Sherry H. Suyu^{2,3,4}, Akın Yıldırım², Eiichiro Komatsu^{2,5}, and José Luis Bernal⁶

- Department of Physics and Astronomy, University of California, Davis, CA 95616, USA e-mail: gcfchen@astro.ucla.edu
- Max Planck Institute for Astrophysics, Karl-Schwarzschild-Strasse 1, 85740 Garching, Germany
- ³ Physik-Department, Technische Universität München, James-Franck-Straße 1, 85748 Garching, Germany
- ⁴ Academia Sinica Institute of Astronomy and Astrophysics (ASIAA), 11F of ASMAB, No. 1, Section 4, Roosevelt Road, Taipei 10617, Taiwan
- ⁵ Kavli IPMU (WPI), UTIAS, The University of Tokyo, Kashiwa, Chiba 277-8583, Japan
- Department of Physics and Astronomy, Johns Hopkins University, 3400 North Charles Street, Baltimore, MD 21218, USA

Received 12 November 2020 / Accepted 26 March 2021

ABSTRACT

Time-delay cosmography with gravitationally lensed quasars plays an important role in anchoring the absolute distance scale and hence measuring the Hubble constant, H_0 , independent of traditional distance ladder methodology. A current potential limitation of time-delay distance measurements is the mass-sheet transformation (MST), which leaves the lensed imaging unchanged but changes the distance measurements and the derived value of H_0 . In this work we show that the standard method of addressing the MST in time-delay cosmography, through a combination of high-resolution imaging and the measurement of the stellar velocity dispersion of the lensing galaxy, depends on the assumption that the ratio, $D_{\rm s}/D_{\rm ds}$, of angular diameter distances to the background quasar and between the lensing galaxy and the quasar can be constrained. This is typically achieved through the assumption of a particular cosmological model. Previous work (TDCOSMO IV) addressed the mass-sheet degeneracy and derived H_0 under the assumption of the Λ CDM model. In this paper we show that the mass-sheet degeneracy can be broken without relying on a specific cosmological model by combining lensing with relative distance indicators such as supernovae Type Ia and baryon acoustic oscillations, which constrain the shape of the expansion history and hence $D_{\rm s}/D_{\rm ds}$. With this approach, we demonstrate that the mass-sheet degeneracy can be constrained in a cosmological model-independent way. Hence model-independent distance measurements in time-delay cosmography under MSTs can be obtained.

Key words. distance scale – gravitational lensing: strong

1. Introduction

The Hubble constant (H_0) is one of the most important parameters in cosmology. Its value directly sets the age, size, and critical density of the Universe. Despite the great success of the Λ cold dark matter (CDM) model (Komatsu et al. 2011; Hinshaw et al. 2013; Planck Collaboration VI 2020), a stringent challenge to the model comes from a discrepancy between the extremely precise H_0 (=67.4 \pm 0.5 km s⁻¹ Mpc⁻¹) value derived from *Planck* measurements of the cosmic microwave background (CMB) anisotropies under the assumption of Λ CDM (Planck Collaboration VI 2020) and the H_0 value from direct measurements of the local Universe (Verde et al. 2019).

The recent direct H_0 measurements ($H_0 = 74.03 \pm 1.42 \, \mathrm{km \, s^{-1} \, Mpc^{-1}}$) from Type Ia supernovae (SN1a), calibrated by the traditional Cepheid distance ladder (SH0ES collaboration; Riess et al. 2019), show a 4.4σ tension with the *Planck* results. However, a recent measurement of $H_0 = 69.8 \pm 0.8 (\mathrm{stat}) \pm 1.7 (\mathrm{sys}) \, \mathrm{km \, s^{-1} \, Mpc^{-1}}$ from SN1a calibrated by the tip of the red giant branch (CCHP) agrees at the 1.2σ level with *Planck* and at the 1.7σ with the SH0ES results (Freedman et al. 2019). The spread in these results, whether due to systematic effects (Efstathiou 2020) or not, clearly demonstrates that it is crucial

to test any single methodology by different and independent datasets.

Time-delay cosmography (TDC; e.g., Treu & Marshall 2016; Suyu et al. 2018) provides a technique to constrain H_0 at low redshift that is completely independent of the traditional distance ladder approach. When a quasar is strongly lensed by a galaxy, its multiple images have light curves that are offset by a well-defined time delay, which depends on the mass profile of the lens and cosmological distances to the galaxy and quasar (Refsdal 1964). A critical aspect of this technique is a model that describes the mass distribution in the lensing galaxy and along the line of sight between the background object and the observer. This model is constrained by the morphology of the lensed emission of the background object, the stellar velocity dispersion in the lensing galaxy, and by deep imaging and spectroscopy of the fields containing the lens system. This model is combined with the time delays (e.g., Bonvin et al. 2018) to measure the characteristic distances for the lens system: the angular diameter distance to the lens (D_d) and the time-delay distance, which is a ratio of the angular diameter distances in the system, as follows:

$$D_{\Delta t} \equiv (1 + z_{\rm d}) \frac{D_{\rm d} D_{\rm s}}{D_{\rm ds}} \propto H_0^{-1},$$
 (1)

where z_d is the redshift of the lens, D_s is the distance to the background source, and D_{ds} is the distance between the lens and the source. In turn, these distances are used to determine cosmological parameters, primarily H_0 (e.g., Suyu et al. 2014; Bonvin et al. 2016; Birrer et al. 2019; Chen et al. 2019; Rusu et al. 2019; Wong et al. 2019; Jee et al. 2019; Taubenberger et al. 2019; Shajib et al. 2020).

A recent analysis with this technique, using a blind analysis on data from six gravitational lens systems¹, inferred $H_0 = 73.3^{+1.7}_{-1.8}\,\mathrm{km\,s^{-1}\,Mpc^{-1}}$, which is a value that was 3.8σ offset from the *Planck* results (Wong et al. 2019; Millon et al. 2020). This analysis used two common descriptions of the mass distribution of the lensing galaxy. The first description consists of a NFW halo (Navarro et al. 1996) plus a constant mass-to-light ratio stellar distribution, called the composite model. The second description models the 3D total mass density distribution, that is, luminous plus dark matter, of the galaxy as a power law (i.e., $\rho(r) \propto r^{-\gamma}$; Barkana 1998); this description is called the power-law model. These models yield H_0 measurements that are consistent within the errors for individual lens systems; the final uncertainties on H_0 incorporate a marginalization over the choice of mass model (Millon et al. 2020).

Although the power-law and composite models are wellmotivated by observations (e.g., Koopmans et al. 2006, 2009; Suyu et al. 2009; Auger et al. 2010; Barnabè et al. 2011; Sonnenfeld et al. 2013; Humphrey & Buote 2010; Cappellari 2016) and simulations (Navarro et al. 1996), there is a wellknown degeneracy in gravitational lensing known as the mass-sheet transformation (MST). The MST leaves imaging observables invariant, but biases the determination of H_0 (Falco et al. 1985; Gorenstein et al. 1988). The line-of-sight mass distribution contributes to first order mass-sheet-like effect (Fassnacht et al. 2002; Suyu et al. 2013; Greene et al. 2013; Collett et al. 2013); we refer to this as an external MST. However, for the mass distribution of the lensing galaxy, there are different models that can give the same lensing observables, but would give different time delays. The most degenerate case is that with spherical symmetry, in which the density profiles differ by a component that is uniform in within the radial ranges probed by lensing. This component, which could be described by a large-core mass distribution (Blum et al. 2020, see detail in Sect. 2), changes the distribution of the mass density profile of the lensing galaxy. This fits with recent works that question whether that elliptical galaxies do not necessarily follow a power-law or composite model to the desired precision (Schneider & Sluse 2013; Xu et al. 2016; Gomer & Williams 2020; Kochanek 2020).

Birrer et al. (2020; hereafter Paper IV) show that allowing for an internal MST on the power-law model increases the uncertainty of the H_0 measurement of a seven-lens sample from the 2.4% precision of Millon et al. (2020) to 8% in a Λ CDM cosmology. Interestingly, the central value of H_0 remained almost unchanged in this analysis (74.5 $^{+5.6}_{-6.1}$ km s⁻¹ Mpc⁻¹). To improve the precision of the H_0 inference, Paper IV added data from the SLACS sample (Bolton et al. 2004, 2006). In this lens sample, the background objects are galaxies, not quasars, so they cannot be used for TDC. However, the combination of high-resolution imaging and kinematic measurements allows the SLACS sample to improve the constraints on the mass profiles of massive elliptical galaxies. With the inclusion of the SLACS information

(Shajib et al. 2021) and the assumption that the sample of time delay and SLACS lenses are drawn from the same population, the inference on H_0 shifted to $67.4^{+4.1}_{-3.2} \,\mathrm{km \, s^{-1} \, Mpc^{-1}}$, which agrees with the Planck value and results from distance ladders (Riess et al. 2019; Freedman et al. 2019). A comparison of the galaxy population distributions shows that several observed properties, such as central stellar velocity dispersion, are similar. In addition, elliptical galaxies are a very homogenous population, as evidenced by the tightness of correlations such as the fundamental plane (Auger et al. 2010, and references therein). However, two major differences between the samples are that the SLACS lensing galaxies are at lower redshifts than those in the time-delay sample and that the SLACS lensing galaxies have smaller ratio of effective radius to Einstein radius than the time-delay sample (see Fig. 16 in Paper IV). Possible potential biases and limitations of using the SLACS sample are discussed by Paper IV and Shajib et al. (2021).

In this work, we take a more general approach to constrain the internal MST by combining the time-delay lens system with relative distance indicators without assuming a specific parametrization of the cosmological model. We show that we can hence constrain the internal MST in a cosmological-independent way and obtain more broadly applicable distance posteriors.

In Sect. 2, we introduce the basics of the MST. In Sects. 3 and 4, we discuss the distance measurements under the effects of the internal and external MST. In Sect. 5, we discuss error propagation under MST. In Sect. 6, we provide a cosmological model-independent way to constrain the internal MST. We summarize our work in Sect. 7.

2. The mass-sheet transformation

The MST is a degeneracy affecting gravitational lens systems. We can transform any projected mass distribution, $\kappa(\theta)$, into infinite sets of $\kappa_{\lambda}(\theta)$ via

$$\kappa_{\lambda}(\theta) = \lambda \kappa(\theta) + 1 - \lambda,$$
(2)

without degrading the fit to the lensed emission (Falco et al. 1985), although MST does change the source size accordingly. In this equation, $\kappa(\theta)$ is a scaled 2D projected mass density distribution, $\kappa(\theta) = \Sigma(\theta)/\Sigma_{crit}$, where $\Sigma(\theta)$ is the mass surface density and Σ_{crit} is the lensing critical density,

$$\Sigma_{\rm cr} = \frac{c^2}{4\pi G} \frac{D_{\rm s}}{D_{\rm d} D_{\rm ds}}.$$
 (3)

The physical picture of MST comes from the environment (a.k.a., an external MST, $\kappa_{\rm ext}$) and the mass models of the lensing galaxy (aka, an internal MST, $\lambda_{\rm int}$). We separate these two components of the MST because we use different observables to assess their effects. For example, the estimation of the external MST uses weighted number counts of galaxies and/or weak gravitational lensing, based on spectroscopy and deep imaging of the field containing the lens. This approach has been extensively used in TDC (e.g., Fassnacht et al. 2006; Suyu et al. 2010; Collett et al. 2013; Greene et al. 2013; Rusu et al. 2017; Tihhonova et al. 2018; Buckley-Geer et al. 2020). Information about the internal MST is derived from high-resolution imaging and the stellar velocity dispersion of the lensing galaxy.

The theoretical version of the internal MST, that is, a mass sheet with infinite extent, is clearly nonphysical. Therefore, in assessing the internal MST we need to find a physical model that approximates the behavior of a mass sheet at small projected distances from the center of the lensing galaxy, but that vanishes

¹ Except the first lens, B1608+656, which was not done blindly, the subsequent five lenses in H0LiCOW are analyzed blindly with respect to the cosmological quantities of interest.

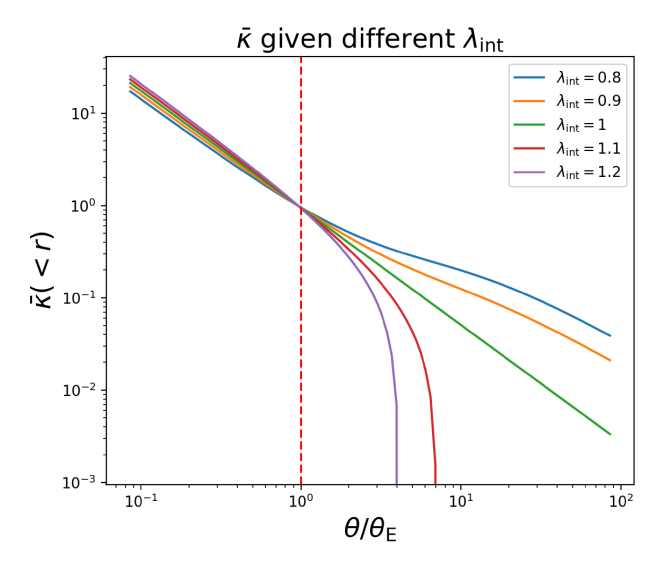


Fig. 1. Illustration of the transformed power-law profile in the mean dimensionless enclosed projected mass distribution under the internal MST with $\theta_s = 10''$. All the transformed mass profiles share the same Einstein radius (red dashed line). All the mass distributions in this figure produce essentially the same model images (i.e., the difference of the χ^2 is less than 0.001%) but a different unlensed size of the source, which is not directly observable.

at large radii (see Fig. 7 in Schneider & Sluse 2013). Effectively, such a mass model redistributes the mass in the region inside the lensed images and in the region outside of the lensed image. This effect, also called monopole degeneracy, was first proposed by Saha (2000) and tested on the real data (e.g., Liesenborgs et al. 2008). Blum et al. (2020) propose a cored mass profile that is also a type of monopole degeneracy. We adopt this cored mass profile to study the impact of the internal MST as it cannot only provide physical 3D mass distribution but also simultaneously satisfy the MST effect.

Given this mass profile, the physical internal MST, which redistributes any specific mass profile, $\kappa(\theta)$, should be written as

$$\kappa_{\text{mst,int}}(\theta) = \lambda_{\text{int}}\kappa(\theta) + (1 - \lambda_{\text{int}})\kappa_{\text{c}}(\theta),$$
(4)

where

$$\kappa_{\rm c}(\theta) = \frac{\theta_{\rm s}}{\sqrt{\theta_{\rm s}^2 + \theta^2}},\tag{5}$$

and θ_s is the scale radius. When we set θ_s to a large value, for example 10", $\kappa_c(\theta)$ approximates the theoretical internal MST very well over the region of interest (Paper IV).

We illustrate the effects of adding such a mass-sheet profile to the lensing galaxy mass distribution in Fig. 1, by plotting the mean dimensionless enclosed projected mass distribution,

$$\bar{\kappa}(\theta) \equiv \frac{2}{\theta^2} \int_0^\theta \theta' \kappa_{\text{mst,int}}(\theta') d\theta'. \tag{6}$$

The Einstein radius of the lens system, θ_E , is defined as the angular radius for which $\bar{\kappa}(\theta_E) = 1$.

Thus, the general MST accounting for both κ_{ext} and λ_{int} can be written as

$$\kappa_{\lambda}(\theta) = (1 - \kappa_{\text{ext}}) \kappa_{\text{mst,int}}(\theta) + \kappa_{\text{ext}} = \kappa_{\text{true}}(\theta),$$
(7)

where κ_{true} represents the true projected mass profile. In this paper we set the stage for future investigations by dissecting

where the constraining power on the distance measurements in TDC comes from and exploring what assumptions have to be made and data have to be used to break the internal MST.

3. Measurement of $D_{\Lambda t}$ under the MST

Once the time delays between multiple images are observed, we can measure the time-delay distance via

$$\Delta t = \frac{D_{\Delta t}}{c} \Delta \phi(\theta, \beta),\tag{8}$$

where c is the speed of light and θ, β , and $\phi(\theta)$ are the image coordinates, source coordinates, and Fermat potential, respectively. The form of Eq. (8) allows the inference of the cosmological information contained in $D_{\Delta t}$ without any need for cosmological priors on the lens modeling.

However, in the presence of a MST, given the same time delays and imaging data, the transformed projected mass profile produces a different time-delay distance via

$$D_{\Delta t,\lambda} = \frac{D_{\Delta t}}{\lambda}.\tag{9}$$

Thus, additional information is required to constrain both the internal and external MST, and thus to obtain unbiased $D_{\Delta t}$ measurements.

4. Measurement of D_d under the MST

Once the velocity dispersion of the lensing galaxy is measured, we can use high-resolution imaging of the lens system to measure the ratio $D_{\rm s}/D_{\rm ds}$ via

$$(\sigma_{\nu}^{p})^{2} = \left(\frac{D_{s}}{D_{ds}}\right) c^{2} J(\eta_{lens}, \eta_{light}, \beta_{ani}), \tag{10}$$

where $\sigma^{\rm p}_{\nu}$ is the predicted line-of-sight luminosity-weighted velocity dispersion that is predicted by the mass distribution in the lensing galaxy. In this equation, J contains the angular-dependent information including the parameters describing the 3D deprojected mass distribution, $\eta_{\rm lens}$, surface-brightness distribution in the lensing galaxy, $\eta_{\rm light}$, and stellar orbital anisotropy distribution, $\beta_{\rm ani}$. In a similar way to the time-delay distance, the separability in Eq. (10) allows us to infer the cosmological distance ratio $D_{\rm s}/D_{\rm ds}$ without the need of cosmological priors on J. Since $D_{\Delta I} \propto D_{\rm d}(D_{\rm s}/D_{\rm ds})$, we can use the combination of the $D_{\Delta I}$ measurement from the time delays and $D_{\rm s}/D_{\rm ds}$ from velocity dispersion to obtain $D_{\rm d}$. We discuss the effect of $\kappa_{\rm ext}$ and $\lambda_{\rm int}$ on the $D_{\rm d}$ measurement in the following two sections.

4.1. External MST only

Jee et al. (2015) find that $D_{\rm d}$ is an invariant quantity under an external MST. This is because $\kappa_{\rm ext}$ only contributes to the change of the normalization of 3D mass profile and does not affect its overall shape given any mass model (Suyu et al. 2013; Chen et al. 2019). That is, the predicted velocity dispersion in Eq. (10) changes to

$$(\sigma_{\nu}^{p})^{2} = (1 - \kappa_{\text{ext}}) \left(\frac{D_{\text{s}}}{D_{\text{ds}}} \right)_{\kappa_{\text{out}}} c^{2} J(\eta_{\text{lens}}, \eta_{\text{light}}, \beta_{\text{ani}}), \tag{11}$$

where the minus sign means that we need to remove the mass contributed from the environment (i.e., the mass along the line of

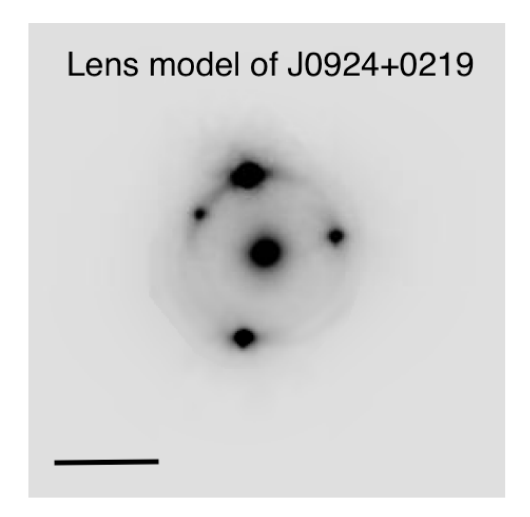


Fig. 2. Multiple lensed images and extended arc around the lensing galaxy from the background AGN and its reconstructed host galaxy. The foreground main lens is located in the center of the lens system. The solid horizontal line represents 1" scale. The detailed lens modeling will be presented in Chen et al. (in prep.). The study of this paper is not limited to any specific configuration of the lens systems.

sight) inside the Einstein radius to obtain the mass of the lensing galaxy.

In order for the predicted velocity dispersion to match the observed value, $D_{\rm s}/D_{\rm ds}$ must transform under an external MST via

$$\left(\frac{D_{\rm s}}{D_{\rm ds}}\right)_{\kappa_{\rm ext}} = (1 - \kappa_{\rm ext})^{-1} \left(\frac{D_{\rm s}}{D_{\rm ds}}\right) = \left(\frac{D_{\rm s}}{D_{\rm ds}}\right)_{\rm true}.$$
 (12)

Then the time-delay distance changes via

$$D_{\Delta t, \kappa_{\text{ext}}} = (1 - \kappa_{\text{ext}})^{-1} D_{\Delta t}. \tag{13}$$

Thus, by combining Eqs. (1), (12), and (13), we can show that D_d is invariant under the external MST,

$$(D_{\rm d})_{\kappa_{\rm ext}} = D_{\rm d}. \tag{14}$$

4.2. Internal MST plus external MST

Since the velocity dispersion depends on the enclosed 3D mass of the lensing galaxy, whose shape is not conserved under an internal MST, the constraint on the $D_{\rm s}/D_{\rm ds}$ ratio is not mathematically scaled by $\lambda_{\rm int}^{-1}$ under an internal MST. We therefore must expand the Eq. (11) by including $\lambda_{\rm int}$ in the J term,

$$(\sigma_{v}^{p})^{2} = (1 - \kappa_{\text{ext}}) \left(\frac{D_{\text{s}}}{D_{\text{ds}}}\right)_{\text{true}} J(\eta_{\text{lens}}, \eta_{\text{light}}, \beta_{\text{ani}}, \lambda_{\text{int}}), \tag{15}$$

since J contains the 3D deprojected dimensionless mass model components, whose structure is affected by the value of λ_{int} . Thus, D_{d} can be expressed as

$$D_{\rm d} = \frac{1}{1 + z_{\rm d}} \frac{D_{\Delta t}}{\lambda_{\rm int}} \frac{c^2}{\sigma_{\nu}^2} J(\eta_{\rm lens}, \eta_{\rm light}, \beta_{\rm ani}, \lambda_{\rm int}). \tag{16}$$

Many previous investigations (e.g., Suyu et al. 2014; Paper IV) show that the internal MST can be broken with a single-aperture velocity dispersion, given a cosmological model. This can be explained as follows: Firstly, the Einstein ring radius, as defined in terms of the mean dimensionless enclosed projected mass distribution (\bar{k}) , is invariant under an internal MST

(i.e., $\bar{\kappa}(\theta_{\rm E}) = \bar{\kappa}_{\lambda}(\theta_{\rm E}) = 1$; see also Fig. 1), while the physical mass inside the Einstein radius is unconstrained without assuming a cosmological model. Secondly, from Eq. (15) we show hereafter that if a cosmological model is not assumed, then the values of $\lambda_{\rm int}$ and $D_{\rm s}/D_{\rm ds}$, which affect the shape and normalization respectively, are degenerate. Hence, even with a measured velocity dispersion, the mass inside the effective radius is also not constrained. Therefore, a single-aperture velocity dispersion is insufficient to break the degeneracy and constrain the internal MST if we do not assume a cosmological model. Spatially resolved kinematics of the lensing galaxy would be required (Yildirim et al., in prep.).

In order to illustrate these dependences, we use the powerlaw mass model, which was obtained by fitting to the real imaging data of a four-image gravitational lens system (J0924+0219) shown in Fig. 2 (see Chen et al., in prep. for details), and analysed this model in the context of an internal MST (i.e., added to our model a MST component as described in Eq. (5)). For the anisotropy component, we assume $\beta_{\rm ani}$ varies with radius and parameterize this behavior in the form of an anisotropy radius, $r_{\rm ani}$, in the Osipkov-Merritt formulation (Osipkov 1979; Merritt 1985),

$$\beta_{\text{ani}} = \frac{r^2}{r_{\text{ani}}^2 + r^2},\tag{17}$$

as an example. In this formulation, $r_{ani} = 0$ indicates pure radial orbits and $r_{\rm ani} \rightarrow \infty$ is isotropic with equal radial and tangential velocity dispersions. In our models, we use a scaled version of the anisotropy parameter, $a_{\rm ani} \equiv r_{\rm ani}/r_{\rm eff}$, where $r_{\rm eff} = D_{\rm d}\theta_{\rm eff}$, and θ_{eff} is the effective radius. The redshift of the lens and source are $z_{\rm d}=0.393$ and $z_{\rm s}=1.523$, respectively. We note that the study of this work is not limited to any specific configuration of the lens systems. We set mock time delays ($\Delta t_{AB} = 10 \pm 1.5$ days, $\Delta t_{\rm CB} = 15 \pm 1.5$ days, $\Delta t_{\rm DB} = 10 \pm 1.5$ days) and a mock velocity dispersion measurement (=279 ± 15 km s⁻¹) for the analysis. The values of mock time delays and the velocity dispersion were chosen to be roughly consistent with the model of J0924 so that they would represent a physically plausible lens. Specifically, given the mass model from the J0924+0219 lens imaging, the mock time delay and velocity dispersion are created by assuming Flat Λ CDM with fixed $\Omega_{\rm m} = 0.3$, $H_0 = 70 \, \rm km \, s^{-1} \, Mpc^{-1}$. and $\lambda_{int} = 1$ (i.e., no internal MST). The uncertainties on the time delays and velocity dispersion are typical of time-delay lens systems. We note that all the figures produced in this work are based on this single lens. Since $\kappa_{\rm ext}$ does not affect the $D_{\rm d}$ measurement and is well understood, we set $\kappa_{\text{ext}} = 0$ throughout the paper for simplicity.

We consider two situations: one with a flat Λ CDM cosmology and another in which we only use the velocity dispersion, time delays, and imaging data without assuming any cosmological model. We note that throughout the paper, for flat Λ CDM cosmology, we assume $\Omega_{\rm m}=[0.05,1.0],\,\Omega_{\Lambda}=1-\Omega_{\rm m}$, and H_0 uniform in $[0,150]\,{\rm km\,s^{-1}\,Mpc^{-1}}$. The results are shown in Fig. 3, where the Λ CDM results are shown as points that are color coded by the velocity dispersion to demonstrate the link between σ_{ν} and the other parameters. Figure 3 clearly demonstrates that $\lambda_{\rm int}$ can be constrained only when Λ CDM is assumed, on the contrary, when the cosmological model constraint is relaxed, $D_{\rm d}$ changes very little within the physically allowed values of $\lambda_{\rm int}$. Thus the J term in Eq. (15) can be very well approximated as $J(\lambda_{\rm int})=\lambda_{\rm int}J$ with <1% shift on the distance measurement of $D_{\rm d}$ for $\theta_{\rm s}=10''$ and with single aperture averaged velocity dispersion. This approximation was also used by Paper IV.

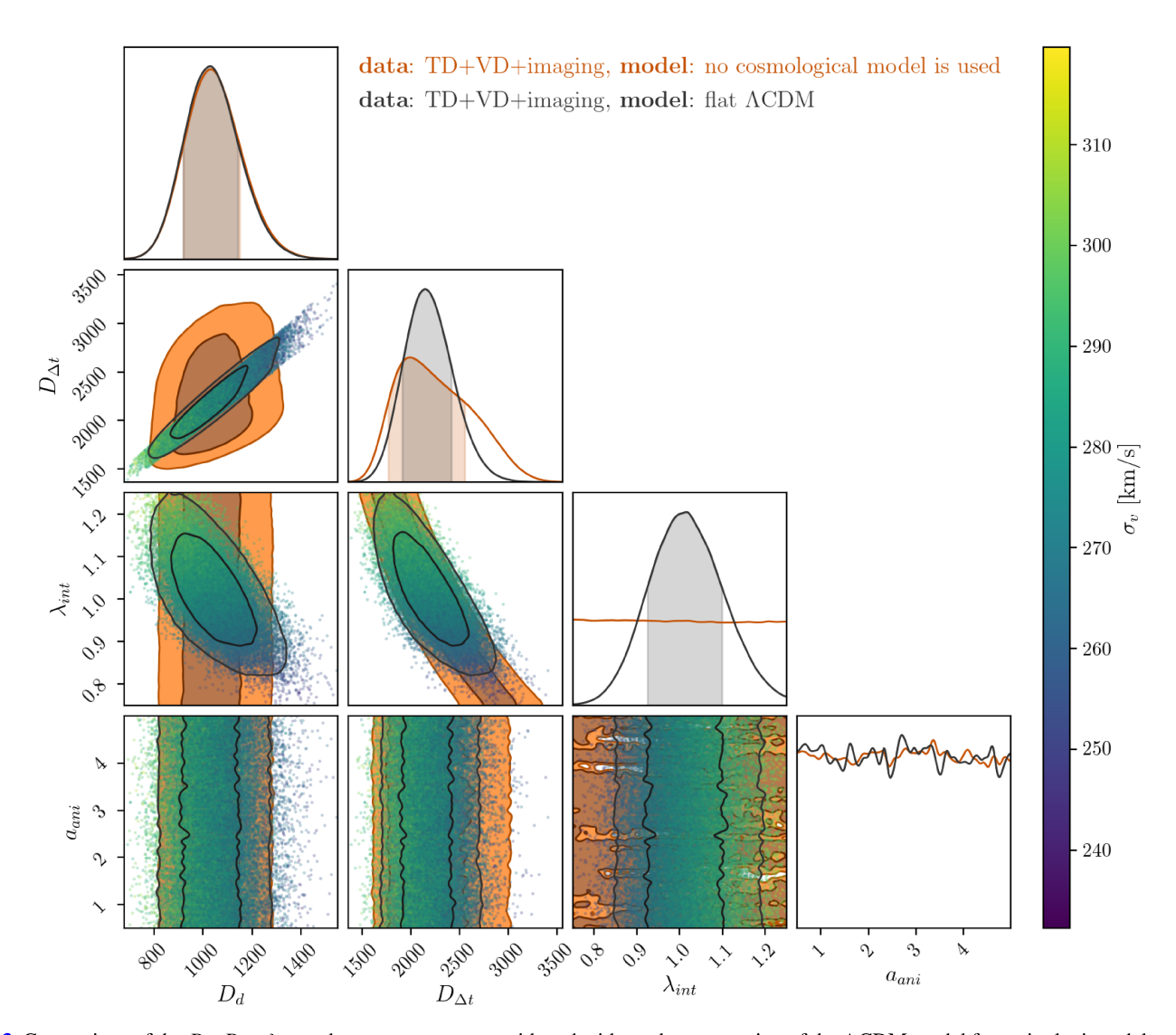


Fig. 3. Comparison of the $D_{\rm d}$, $D_{\Delta t}$, $\lambda_{\rm int}$, and $a_{\rm ani}$ measurements with and without the assumption of the $\Lambda{\rm CDM}$ model from single time-delay mock lens. The abbreviation "TD" represents time-delay information and "VD" represents velocity dispersion information. When $\Lambda{\rm CDM}$ model is not assumed, the internal MST ($\lambda_{\rm int}$) is not constrained. When $\Lambda{\rm CDM}$ model is assumed, the degeneracy can be broken and hence $D_{\Delta t}$ is constrained. The anisotropy parameter is not constrained in either case. Color-coded velocity dispersion shows that $D_{\Delta t}$ is positively correlated with $D_{\rm d}$ but anticorrelated with σ_v . The contours represent the 68.3% (shaded region) and 95.4% quantiles.

5. Error propagation in MST

5.1. Error propagation without assuming a cosmological

In the previous section, we showed that $D_{\Delta t}$ is directly affected by both external and internal MST, while $D_{\rm d}$ is not affected by $\kappa_{\rm ext}$ and is nearly invariant. Thus, based on Eq. (9) the error on $D_{\Delta t}$ ($\delta D_{\Delta t}$) given λ and $\lambda_{\rm int}$ scales as

$$\frac{\delta D_{\Delta t}}{D_{\Delta t}} \sim -\frac{\delta \lambda}{\lambda} = -\frac{\delta \lambda_{\text{int}}}{\lambda_{\text{int}}},\tag{18}$$

while based on Eq. (16), the error of D_d scales as

$$\frac{\delta D_{\rm d}}{D_{\rm d}} \sim -2 \frac{\delta \sigma_{\nu}}{\sigma_{\nu}},\tag{19}$$

where σ_{ν} is the measured line-of-sight velocity dispersion. Thus, the uncertainties on $D_{\rm d}$ are dominated by the velocity dispersion measurement errors, while the $D_{\Delta t}$ uncertainties are dominated

by both internal and external MST. Therefore, H_0 inferred solely from D_d is robust against the MST (Jee et al. 2019)².

5.2. Error propagation under ΛCDM model

However, if one assumes a ΛCDM model, the error on λ_{int} is written as

$$\frac{\delta \lambda_{\rm int}}{\lambda_{\rm int}} \sim 2 \frac{\delta \sigma_{\nu}}{\sigma_{\nu}}.$$
 (20)

By combining Eqs. (18)–(20), the correlations between the errors on $D_{\Delta t}$, $D_{\rm d}$, and $\sigma_{\rm v}$ are given by

$$\frac{\delta D_{\Delta t}}{D_{\Delta t}} \sim \frac{\delta D_{\rm d}}{D_{\rm d}} \sim -2 \frac{\delta \sigma_{\nu}}{\sigma_{\nu}}.$$
 (21)

In Fig. 3, we see that under the assumption of the Λ CDM model, $D_{\Delta t}$ is positively correlated with $D_{\rm d}$ but anticorrelated with σ_{ν} .

² We note that Jee et al. (2019) shows that different anisotropy model may slightly shift the inferred D_d value.

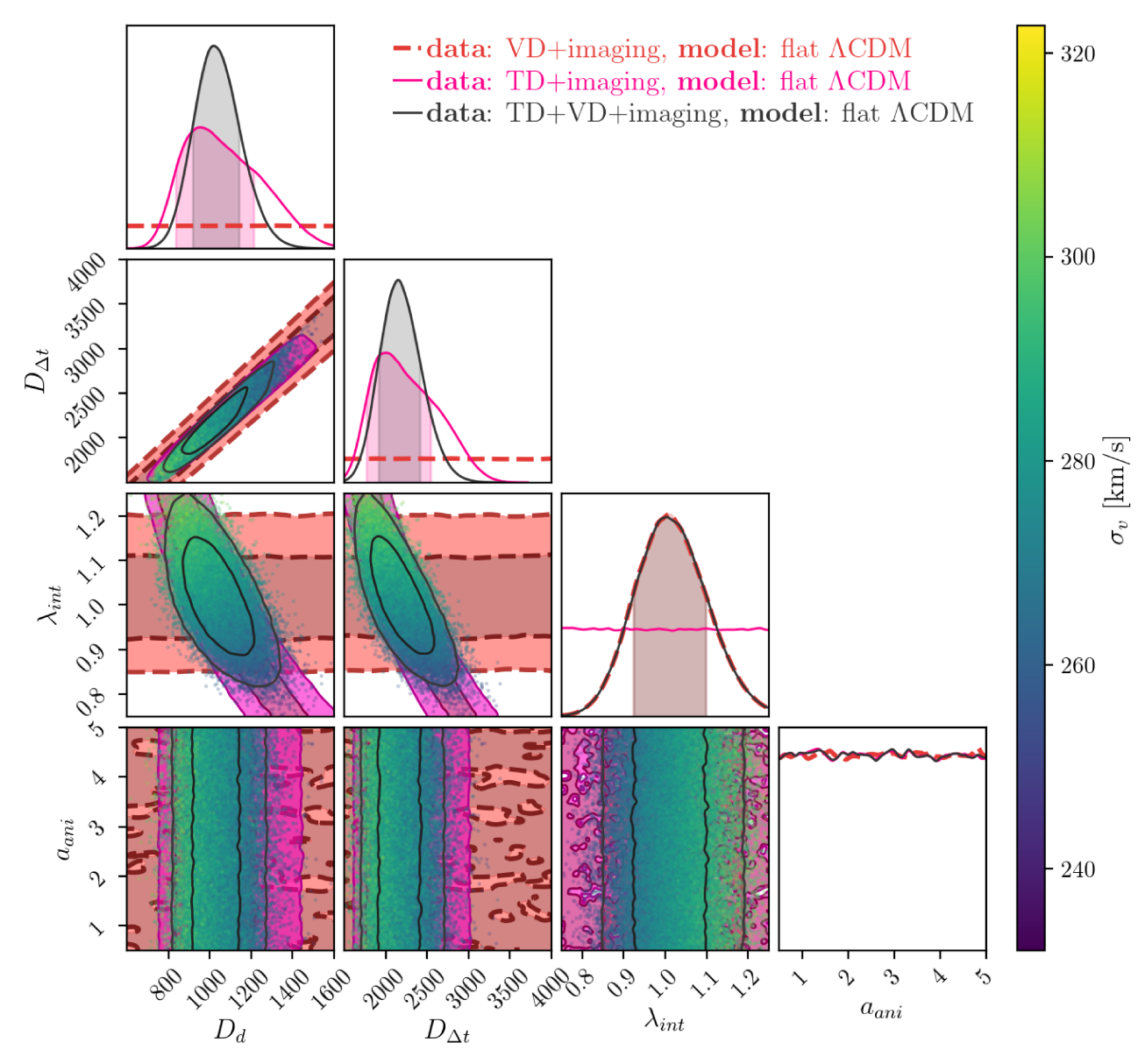


Fig. 4. Decomposition of the constraining power from time delays (TD), velocity dispersion (VD), and imaging data under the assumption of the Λ CDM model. When only "TD+imaging" is used, the values of $D_{\rm d}$ and $D_{\Delta t}$ are not constrained, and both of them are fully degenerate with $\lambda_{\rm int}$. Since the velocity dispersion constrains the $\lambda_{\rm int}$, the joint constraint ("TD+VD+imaging data") breaks the degeneracy and hence constrains $D_{\Delta t}$ and $D_{\rm d}$. The anisotropy parameters are not constrained in all cases.

Most importantly, while Eqs. (20) and (21) tell us that $D_{\Delta t}$ and $D_{\rm d}$ are anticorrelated with $\lambda_{\rm int}$ under Λ CDM model, $D_{\rm d}$ is nearly uncorrelated with $\lambda_{\rm int}$ without assuming a cosmological model inside the physically allowed range of $\lambda_{\rm int}$.

6. Constraining the internal MST

In the previous sections of this paper, we have shown that in the presence of an internal MST, parameterized by $\lambda_{\rm int}$, the time-delay distance measurement is poorly constrained unless a specific cosmological model is picked. This situation is clearly demonstrated in the $\lambda_{\rm int}$ versus $D_{\Delta t}$ panel in Fig. 3, where $\lambda_{\rm int}$ is essentially unconstrained without the assumption of a cosmological model. In turn, the large uncertainties in $\lambda_{\rm int}$ translate into imprecise inferences on $D_{\Delta t}$. Therefore, in this section we describe two approaches to improving the constraints on $\lambda_{\rm int}$. The first approach constrains $\lambda_{\rm int}$ in a fashion that depends on

the cosmological model (Paper IV), while the second approach works even if we are agnostic about the cosmological model. In both cases, we assume that observations have provided measurements of time delays and luminosity-weighted stellar velocity dispersions with errors that are typical of those found in previous works in this field.

6.1. Method 1: Choosing a cosmological model

In Sect. 4.2, we demonstrated that $D_{\rm s}/D_{\rm ds}$ and $\lambda_{\rm int}$ are degenerate quantities. However, once a cosmological model is assumed, $D_{\rm s}/D_{\rm ds}$ can be determined up to a range depending on the other cosmological parameters such as $\Omega_{\rm m}$ and Ω_k (Grillo et al. 2008), since the unknown factor of H_0 cancels out in the ratio. This means that the measurement of the velocity dispersion constrains $\lambda_{\rm int}$, hence the mass inside the effective radius of the lensing galaxy. Once $\lambda_{\rm int}$ is constrained, $D_{\Delta t}$ is constrained and $D_{\rm d}$ can

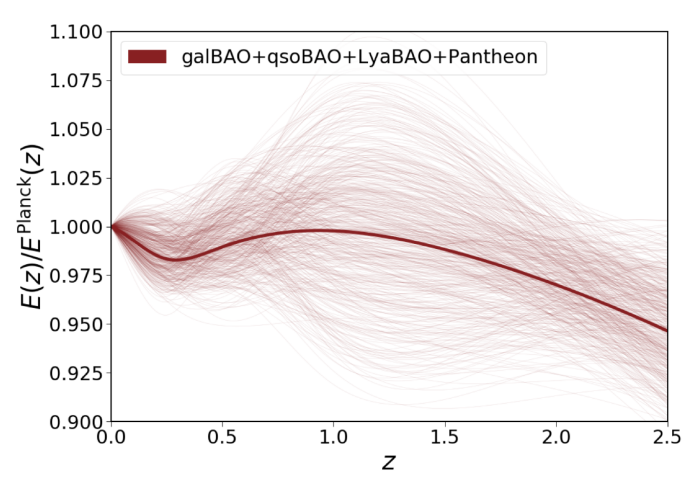


Fig. 5. Results of the reconstruction of E(z) (= $H(z)/H_0$) using the SN1a and BAO data, normalized by the values for our fiducial cosmology given by the best-fitting parameters from the *Planck* analysis for a Λ CDM model. Each thin line comes from a random draw among the points in parameter space within 68% confidence level. The thick line in the middle represents the best fit. The uncertainties are relatively large at z=1-1.5 since the error bars of the Baryon acoustic oscillations (BAO) measurements at z=0.8, and especially, at z=1.5, are significantly larger, while SN1a measurements are only powerful enough to constrain the splines at $z\sim0.8-1$. The shape of expansion history is described by piecewise natural cubic splines. The splines constrained by the data can be used to constrain D_s/D_{ds} and hence break the internal MST.

be inferred from $D_{\Delta t}$. Hence the mass inside the Einstein radius is assigned. Therefore, by assuming a cosmological model, the internal MST can be broken to a level that depends on the precision of the velocity dispersion measurement. To further illustrate the effect of assuming a cosmological model, we show the constraining power on $D_{\rm d}$, $D_{\Delta t}$, $\lambda_{\rm int}$, and the anisotropy parameter $(a_{\rm ani})$ when setting the cosmological model to $\Lambda{\rm CDM}$ in Fig. 3. We clearly see the correlation between $D_{\Delta t}$ and inferred $D_{\rm d}$ under the assumption of the $\Lambda{\rm CDM}$.

For the case in which no cosmological model is used in Fig. 3, we see that $D_{\Delta t}$ is degenerate with $\lambda_{\rm int}$. In contrast, by assuming a cosmological model, we restrict the allowed range of $\lambda_{\rm int}$ and this places stronger constraints on the inferences on the cosmological distances. We can decompose the black contour in Fig. 3 into separate cases to examine the constraining power from the velocity dispersion only (VD only), time-delay measurements only (TD only), and a joint constraint from both measurements (VD plus TD). Figure 4 clearly shows that the velocity dispersion constrains $\lambda_{\rm int}$ when assuming a cosmological model (e.g., Λ CDM). In other words, the value of $\lambda_{\rm int}$ depends on the cosmological model and the measurement of $D_{\Delta t}$ in this case is not a cosmological model-independent quantity.

6.2. Method 2: Using external datasets to constrain D_s/D_{ds}

To break the internal MST without assuming a particular cosmological model (e.g., Λ CDM model), we require additional information to constrain $D_{\rm s}/D_{\rm ds}$. This can be done by including data on SN1a and BAO). The SN1a data are given as measurements of the distance modulus

$$\mu(z) \equiv m - M = 25 + 5\log_{10}D_L(z),\tag{22}$$

where m is the apparent magnitude, M is a fiducial absolute magnitude, and D_L is the luminosity distance. When M is a free

Table 1. Summary of the BAO measurements that are used in this work.

Measurement	Zeff	Reference
$r_{ m s}/D_V$	0.106	Beutler et al. (2011)
$D_V/r_{ m s}$	0.15	Ross et al. (2015)
$D_M(r_{\rm s,fid}/r_{\rm s})$ (Mpc)	0.38	Alam et al. (2017)
$H(z)(r_{\rm s}/r_{\rm s,fid}) ({\rm km s^{-1} Mpc^{-1}})$	0.38	
$D_M(r_{\rm s,fid}/r_{\rm s})$ (Mpc)	0.51	
$H(z)(r_{\rm s}/r_{\rm s,fid}) ({\rm km s^{-1} Mpc^{-1}})$	0.51	
$D_M(r_{\rm s,fid}/r_{\rm s})$ (Mpc)	0.61	
$H(z)(r_{\rm s}/r_{\rm s,fid}) ({\rm km s^{-1} Mpc^{-1}})$	0.61	
$D_V/r_{ m s}$	0.44	Kazin et al. (2014)
$D_V/r_{ m s}$	0.6	
$D_V/r_{ m s}$	0.73	
$D_M/r_{ m s}$	0.698	Gil-Marín et al. (2020)
$c/(H(z)*r_{\rm s})$	0.698	
$D_M/r_{ m s}$	1.48	Hou et al. (2021) and Neveux et al. (2020)
$c/(H(z)*r_s)$	1.48	
$D_M/r_{ m s}$	2.33	du Mas des Bourboux et al. (2020)
$c/(H(z)*r_{\rm s})$	2.33	

Notes. In our fiducial cosmology, $r_{s,fid} = 147.78 \,\mathrm{Mpc}$.

parameter without calibration, SN1a only constrain the shape of the expansion history. The BAO data provide measurements of $D_V/r_{\rm s}$, the dilation scale normalized by the standard ruler length (or $D_A/r_{\rm s}$ and $Hr_{\rm s}$ in the anisotropic analysis), where

$$D_V \equiv \left[D_M^2(z) \frac{cz}{H(z)} \right]^{1/3},\tag{23}$$

 $D_M = (1+z)D_A$, and D_A is the angular diameter distance. If we vary M and r_s freely, those data sets provide the information on the shape of the expansion history (e.g., Cuesta et al. 2015) and thus D_s/D_{ds} .

However, we still require a model for the redshift distance relationship to connect these data. In this work, we choose piecewise natural cubic splines³ to describe H(z) that fit to the data. The spline method has been used in many studies to reconstruct the expansion history (Bernal et al. 2016, 2019; Poulin et al. 2018; Aylor et al. 2019). The splines are set by the values they take at different redshifts. These values can uniquely define the piecewise cubic spline once we require continuity of H(z) and its first and second derivatives at the knots, and set two boundary conditions. We also require the second derivative to vanish at the exterior knots. We set the minimal assumptions of this work: (1) cosmological principle of homogeneity and isotropy (i.e., Friedmann-Lemaître-Robertson-Walker metric); (2) assumption of general relativity: the curvature density parameter is given by $\Omega_k = k[c/(R_0H_0)]^2$ where $k = \{1, 0, -1\}$, R_0 denotes the present value of the scale factor; (3) spline H(z) completely specifies the FLRW metric; and (4) cosmic distance duality relation: $D_L = D_A (1+z)^2$.

To get a good constraint on the cosmological model-independent $D_{\rm s}/D_{\rm ds}$ at the redshift of the mock lens, we need the data that cover the redshift up to the source redshift⁴ ($z_{\rm s}=1.523$ in this case). Current existing data show that we can constrain the shape of the expansion history up to $\sim z=2.5$ (see Fig. 3 in Bernal et al. 2019). Therefore, we update

³ We note that linear interpolation (e.g., Verde et al. 2017), Gaussian processes (e.g., Joudaki et al. 2018; Liao et al. 2020), or smooth Taylor expansion (e.g., Macaulay et al. 2019; Wojtak & Agnello 2019; Arendse et al. 2020) are alternatives.

⁴ For the current seven TDCOSMO lenses, the source redshifts are all below $z_s = 2.5$.

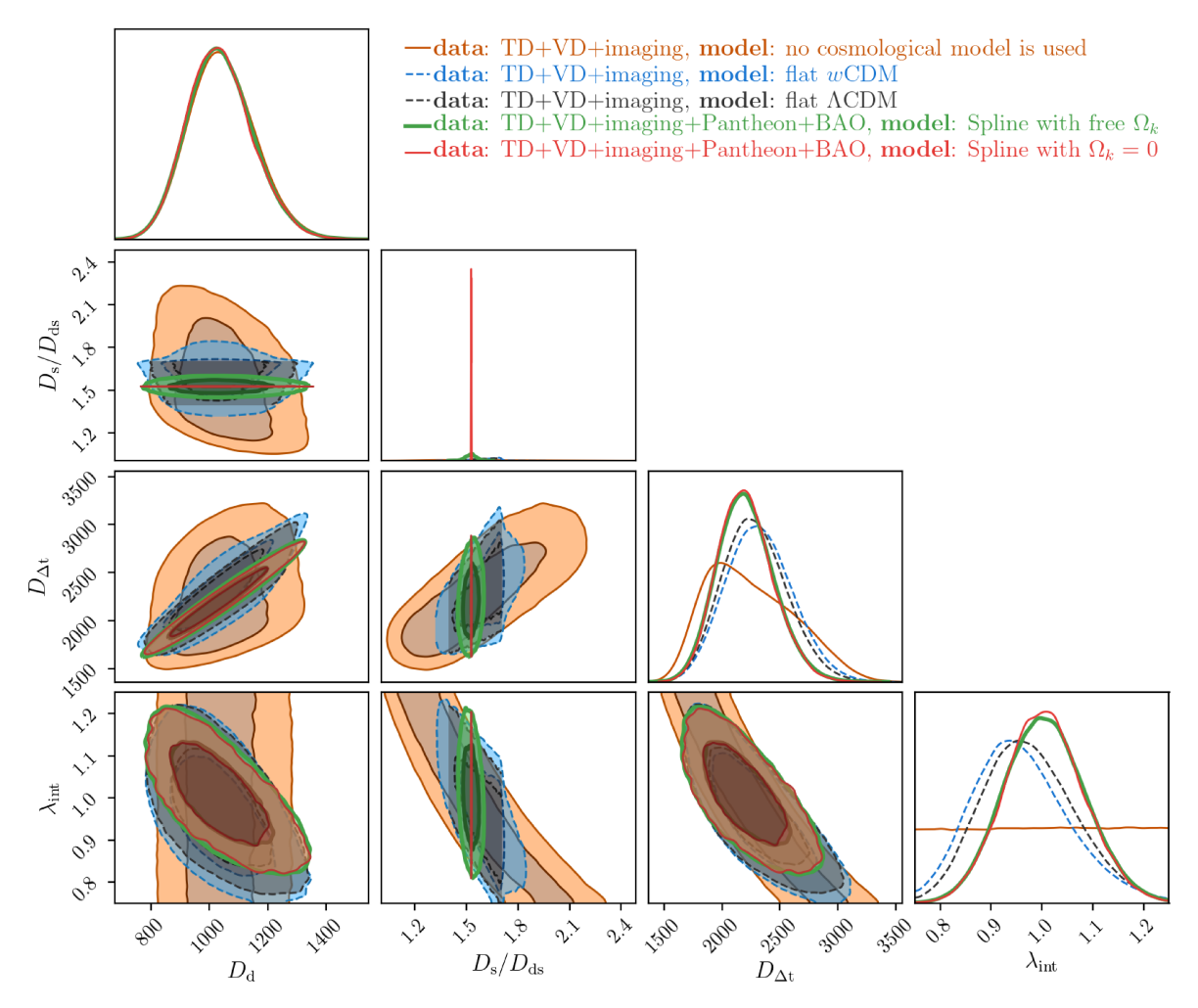


Fig. 6. Comparison of the inferred D_d , D_s/D_{ds} , $D_{\Delta t}$, and λ_{int} in different cases. Case 1 (orange): The distance measurements directly from single time-delay mock lens without assuming any cosmological model. Case 2 (blue): The distance measurements under the assumption of the flat wCDM model with $\Omega_m = [0.05, 1.0]$, $\Omega_{dc} = 1 - \Omega_m$, w = [-2.5, 0.5], and H_0 uniform in [0, 150] km s⁻¹ Mpc⁻¹. Case 3 (black): The distance measurements under the assumption of the Λ CDM model with $\Omega_m = [0.05, 1.0]$, $\Omega_{\Lambda} = 1 - \Omega_m$, and H_0 uniform in [0, 150] km s⁻¹ Mpc⁻¹. Case 4: (green): The distance measurements from single time-delay mock lens, Pantheon dataset, and BAO dataset by using splines with free Ω_k . Case 5 (red): The distance measurements from single time-delay mock lens, Pantheon dataset, and BAO dataset by using splines with $\Omega_k = 0$. For the cases (green and red) that do not assume a particular cosmological model, the constraining power on λ_{int} is comparable to the cases (blue and black) with an assumption of having a underlying cosmological model.

the likelihood used in Bernal et al. (2019) and use the Pantheon datasets of SN1a (Scolnic et al. 2018), BAO from galaxies (Kazin et al. 2014; Alam et al. 2017; Gil-Marín et al. 2020), quasars (Hou et al. 2021; Neveux et al. 2020), and the Lyman- α forest (du Mas des Bourboux et al. 2020). For the eBOSS likelihoods, we use the Gaussian approximation and that BAO can be used to apply cosmological models beyond LCDM (Bernal et al. 2020; Carter et al. 2020). We summarize the BAO measurements and the redshift information in Table 1. We set five "knots" at different redshifts ($z_0 = 0$, $z_1 = 0.25$, $z_2 = 0.5$, $z_3 = 1$., $z_4 = 2.5$). The complete set of parameters for the Spline model is $\{H_0, H_1, H_2, H_3, H_4, r_s, \Omega_k, M\}$. Uniform priors are assumed for all parameters. We show the reconstructed $E(z)(=H(z)/H_0)$ normalised by the values for our fiducial cosmology given by the best-fitting parameters from the Planck analysis for a ACDM model in Fig. 5. The posterior of D_s/D_{ds} can be obtained by integrating E(z).

In Fig. 6, we show that by combining the inference from the external datasets on $H(z)/H_0$, which constrain D_s/D_{ds} , with time-delay strong lensing systems, we can obtain cosmological

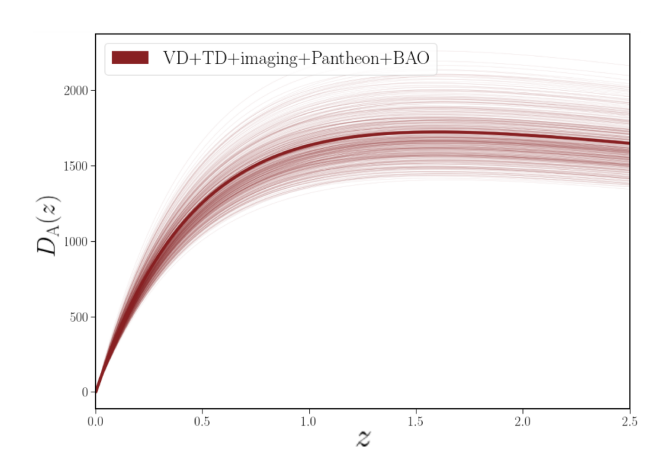


Fig. 7. Cosmological model-independent distance measurements from combining single time-delay mock lens with Pantheon and BAO datasets. Each thin line comes from a random draw among the points in parameter space within 68% confidence level. The thick line in the middle represents the best fit.

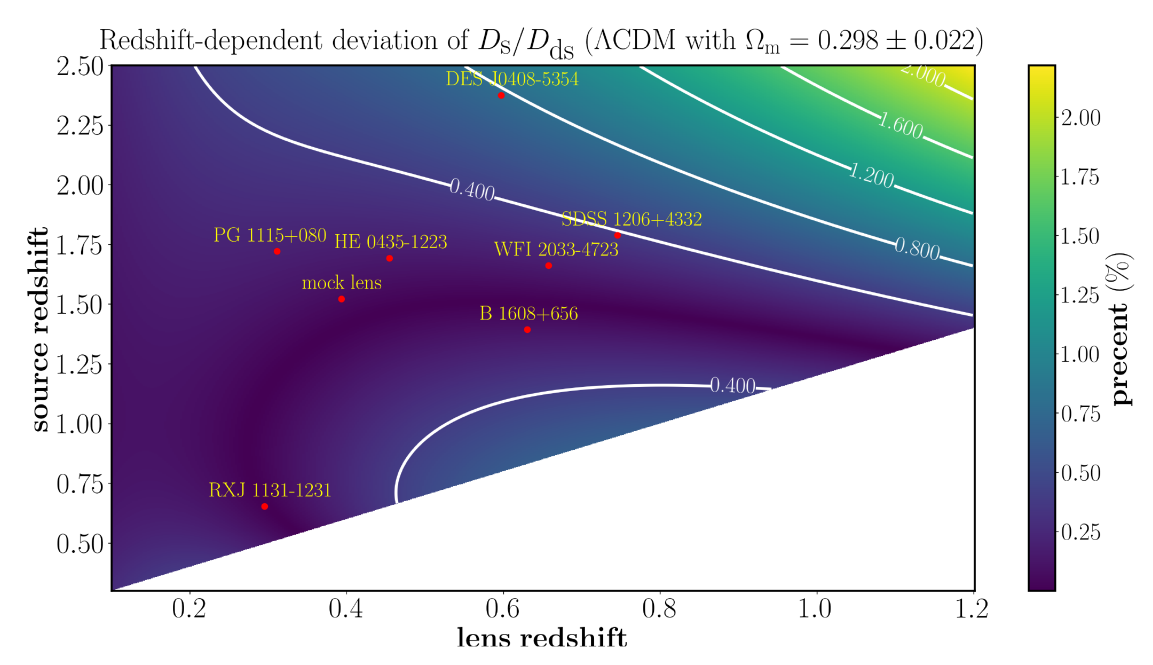


Fig. 8. Percent difference between the median value of D_s/D_{ds} , directly constrained from the SN1a and BAO, and the D_s/D_{ds} under the assumption of the Λ CDM model with $\Omega_{\rm m}=0.298\pm0.022$ (Scolnic et al. 2018), which was used in Paper IV. All 7 time-delay lenses show <1% deviation validate the use of the Pantheon datasets that constrain the low-redshift expansion history and the use of Λ CDM model that extrapolates the constraint on D_s/D_{ds} at high redshift.

model-independent $D_{\rm d}$ and $D_{\Delta t}$ measurements that are comparable to those obtained by assuming a $\Lambda {\rm CDM}$ or $w{\rm CDM}$ cosmology. In addition, we also see that the values of $\lambda_{\rm int}$ under $\Lambda {\rm CDM}$ and $w{\rm CDM}$ are slightly offset from the cases that include SN1a and BAO datasets. This is because the flat priors on $\Omega_{\rm m}$ and w in $\Lambda {\rm CDM}$ and $w{\rm CDM}$ models do not reflect the expansion history described by the SN1a and BAO datasets. Thus, it indicates the importance of including the external datasets, which directly constrain the expansion history to get distance measurements.

In Fig. 7, we show the distance measurements from combining a single time-delay lens with SN1a and BAO with free Ω_k (the green contour in Fig. 6). This distance measurements can be used to infer H_0 in generic cosmological models. We emphasize that this approach does not require the absolute calibration of SN1a or BAO; thus, the derived constraint on H_0 remains independent of the distance ladder and the sound horizon scale.

6.3. Comparison with Paper IV

In the previous section, we demonstrate that D_s/D_{ds} is fully degenerate with λ_{int} , which affects the time-delay distance measurement. Therefore, we compare the redshift-dependent median value of D_s/D_{ds} , constrained directly by the SN and BAO data at the redshift of the current seven TDCOSMO lens samples, with the D_s/D_{ds} in Paper IV, which used the prior based on Pantheon sample with $\Omega_{\rm m} = 0.298 \pm 0.022$ (Scolnic et al. 2018) under the assumption of the ACDM model. These results shown in Fig. 8 demonstrate that in the case of these seven lenses, using the prior information from Pantheon datasets that constrain the low redshift expansion history and then using Λ CDM model to extrapolate the constraint on D_s/D_{ds} to high redshift are valid approaches, because the deviations from the median value of D_s/D_{ds} are all below 1%, thereby demonstrating that the shape of the expansion history is described well by the Λ CDM model. However, the time-delay distance measurements derived by the method developed in this work are broadly applicable distance

posteriors, which can be used to infer H_0 in various cosmological models.

7. Conclusions

In this work, we use a mock gravitational lens system to study the correlation between distance measurements under the MST with or without assuming a cosmological model. We verify that although $D_{\Delta t}$ is directly correlated with both the internal and external MST, D_d is not only invariant under an external MST but is also insensitive to the internal MST. Thus, without assuming any particular cosmological model, the role of velocity dispersion is to obtain the angular diameter distance to the lens (D_d) rather than break the internal MST (λ_{int}) . To break λ_{int} , in addition to the velocity dispersion, we identify that constraining D_s/D_{ds} is the key, which is typically achieved through the assumption of a particular cosmological model, and hence λ_{int} and $D_{\Delta t}$ are both cosmological-model-dependent quantities. In this work, we show that cosmological model-independent $D_{\Delta t}$ measurement can be achieved when relative distance indicators (e.g., SN1a and BAO) are used to constrain D_s/D_{ds} and hence λ_{int} . These distance measurements with SN1a and BAO shown in Fig. 7 can then be used to infer H_0 in generic cosmological models. It is important to stress that this approach does not require the absolute calibration of SN1a or BAO; thus, the derived constraint on H_0 remains independent⁵ of the distance ladder and the sound horizon scale.

Acknowledgements. GC-FC thanks Simon Birrer, Adriano Agnello, James Chan, Tommaso Treu, Dominique Sluse, Matt Auger, and Elizabeth Buckley-Geer for many insightful comments. GC-FC thanks Alessandro Sonnenfeld for useful suggestions on using stellar kinematics code and Ken Wong for the code review. GC-FC acknowledges support by NSF through grants NSF-AST-1906976 and NSF-AST-1836016. GC-FC acknowledges support from the Moore Foundation through grant 8548. GC-FC and CDF acknowledge support for this

⁵ https://github.com/astrosonnen/spherical_jeans

work from the National Science Foundation under Grant Nos. AST-171561 and AST-1907396. SHS and AY thank the Max Planck Society for support through the Max Planck Research Group for SHS. SHS and EK are supported in part by the Deutsche Forschungsgemeinschaft (DFG, German Research Foundation) under Germany's Excellence Strategy – EXC-2094 – 390783311. The Kavli IPMU is supported by World Premier International Research Center Initiative (WPI), MEXT, Japan. J. L. B. is supported by the Allan C. and Dorothy H. Davis Fellowship.

References

```
Alam, S., Ata, M., Bailey, S., et al. 2017, MNRAS, 470, 2617
Arendse, N., Wojtak, R. J., Agnello, A., et al. 2020, A&A, 639, A57
Auger, M. W., Treu, T., Bolton, A. S., et al. 2010, ApJ, 724, 511
Aylor, K., Joy, M., Knox, L., et al. 2019, ApJ, 874, 4
Barkana, R. 1998, ApJ, 502, 531
Barnabè, M., Czoske, O., Koopmans, L. V. E., Treu, T., & Bolton, A. S. 2011,
   MNRAS, 415, 2215
Bernal, J. L., Verde, L., & Riess, A. G. 2016, JCAP, 10, 019
Bernal, J. L., Breysse, P. C., & Kovetz, E. D. 2019, Phys. Rev. Lett., 123, 251301
Bernal, J. L., Smith, T. L., Boddy, K. K., & Kamionkowski, M. 2020, Phys. Rev.
   D. 102, 123515
Beutler, F., Blake, C., Colless, M., et al. 2011, MNRAS, 416, 3017
Birrer, S., Treu, T., Rusu, C. E., et al. 2019, MNRAS, 484, 4726
Birrer, S., Shajib, A. J., Galan, A., et al. 2020, A&A, 643, A165
Blum, K., Castorina, E., & Simonović, M. 2020, ApJ, 892, L27
Bolton, A. S., Burles, S., Schlegel, D. J., Eisenstein, D. J., & Brinkmann, J. 2004,
   AJ, 127, 1860
Bolton, A. S., Burles, S., Koopmans, L. V. E., Treu, T., & Moustakas, L. A. 2006,
Bonvin, V., Tewes, M., Courbin, F., et al. 2016, A&A, 585, A88
Bonvin, V., Chan, J. H. H., Millon, M., et al. 2018, A&A, 616, A183
Buckley-Geer, E. J., Lin, H., Rusu, C. E., et al. 2020, MNRAS, 498, 3241
Cappellari, M. 2016, ARA&A, 54, 597
Carter, P., Beutler, F., Percival, W. J., et al. 2020, MNRAS, 494, 2076
Chen, G. C. F., Fassnacht, C. D., Suyu, S. H., et al. 2019, MNRAS, 2193
Collett, T. E., Marshall, P. J., Auger, M. W., et al. 2013, MNRAS, 432, 679
Cuesta, A. J., Verde, L., Riess, A., & Jimenez, R. 2015, MNRAS, 448, 3463
du Mas des Bourboux, H., Rich, J., Font-Ribera, A., et al. 2020, ApJ, 901, 153
Efstathiou, G. 2020, ArXiv e-prints [arXiv:2007.10716]
Falco, E. E., Gorenstein, M. V., & Shapiro, I. I. 1985, ApJ, 289, L1
Fassnacht, C. D., Xanthopoulos, E., Koopmans, L. V. E., & Rusin, D. 2002, ApJ,
   581, 823
Fassnacht, C. D., Gal, R. R., Lubin, L. M., et al. 2006, ApJ, 642, 30
Freedman, W. L., Madore, B. F., Hatt, D., et al. 2019, ApJ, 882, 34
Gil-Marín, H., Bautista, J. E., Paviot, R., et al. 2020, MNRAS, 498, 2492
Gomer, M., & Williams, L. L. R. 2020, JCAP, 2020, 045
Gorenstein, M. V., Falco, E. E., & Shapiro, I. I. 1988, ApJ, 327, 693
Greene, Z. S., Suyu, S. H., Treu, T., et al. 2013, ApJ, 768, 39
Grillo, C., Lombardi, M., & Bertin, G. 2008, A&A, 477, 397
```

```
Hinshaw, G., Larson, D., Komatsu, E., et al. 2013, ApJS, 208, 19
Hou, J., Sánchez, A. G., Ross, A. J., et al. 2021, MNRAS, 500, 1201
Humphrey, P. J., & Buote, D. A. 2010, MNRAS, 403, 2143
Jee, I., Komatsu, E., & Suyu, S. H. 2015, JCAP, 11, 033
Jee, I., Suyu, S. H., Komatsu, E., et al. 2019, Science, 365, 1134
Joudaki, S., Kaplinghat, M., Keeley, R., & Kirkby, D. 2018, Phys. Rev. D, 97,
Kazin, E. A., Koda, J., Blake, C., et al. 2014, MNRAS, 441, 3524
Kochanek, C. S. 2020, MNRAS, 493, 1725
Komatsu, E., Smith, K. M., Dunkley, J., et al. 2011, ApJS, 192, 18
Koopmans, L. V. E., Treu, T., Bolton, A. S., Burles, S., & Moustakas, L. A. 2006,
   ApJ, 649, 599
Koopmans, L. V. E., Bolton, A., Treu, T., et al. 2009, ApJ, 703, L51
Liao, K., Shafieloo, A., Keeley, R. E., & Linder, E. V. 2020, ApJ, 895, L29
Liesenborgs, J., de Rijcke, S., Dejonghe, H., & Bekaert, P. 2008, MNRAS, 389,
Macaulay, E., Nichol, R.C., Bacon, D., et al. 2019, MNRAS, 966
Merritt, D. 1985, AJ, 90, 1027
Millon, M., Galan, A., Courbin, F., et al. 2020, A&A, 639, A101
Navarro, J. F., Frenk, C. S., & White, S. D. M. 1996, ApJ, 462, 563
Neveux, R., Burtin, E., de Mattia, A., et al. 2020, MNRAS, 499, 210
Osipkov, L. P. 1979, Pis ma Astronomicheskii Zhurnal, 5, 77
Planck Collaboration VI. 2020, A&A, 641, A6
Poulin, V., Boddy, K. K., Bird, S., & Kamionkowski, M. 2018, Phys. Rev. D, 97,
   123504
Refsdal, S. 1964, MNRAS, 128, 307
Riess, A. G., Casertano, S., Yuan, W., Macri, L. M., & Scolnic, D. 2019, ApJ,
Ross, A. J., Samushia, L., Howlett, C., et al. 2015, MNRAS, 449, 835
Rusu, C. E., Fassnacht, C. D., Sluse, D., et al. 2017, MNRAS, 467, 4220
Rusu, C. E., Wong, K. C., Bonvin, V., et al. 2019, MNRAS, 498, 1440
Saha, P. 2000, AJ, 120, 1654
Schneider, P., & Sluse, D. 2013, A&A, 559, A37
Scolnic, D. M., Jones, D. O., Rest, A., et al. 2018, ApJ, 859, 101
Shajib, A. J., Birrer, S., Treu, T., et al. 2020, MNRAS, 494, 6072
Shajib, A. J., Treu, T., Birrer, S., & Sonnenfeld, A. 2021, MNRAS, 503, 2380
Sonnenfeld, A., Treu, T., Gavazzi, R., et al. 2013, ApJ, 777, 98
Suyu, S. H., Marshall, P. J., Blandford, R. D., et al. 2009, ApJ, 691, 277
Suyu, S. H., Marshall, P. J., Auger, M. W., et al. 2010, ApJ, 711, 201
Suyu, S. H., Auger, M. W., Hilbert, S., et al. 2013, ApJ, 766, 70
Suyu, S. H., Treu, T., Hilbert, S., et al. 2014, ApJ, 788, L35
Suyu, S. H., Chang, T.-C., Courbin, F., & Okumura, T. 2018, Space Sci. Rev.,
Taubenberger, S., Suyu, S. H., Komatsu, E., et al. 2019, A&A, 628, L7
Tihhonova, O., Courbin, F., Harvey, D., et al. 2018, MNRAS, 477, 5657
Treu, T., & Marshall, P. J. 2016, A&ARv, 24, 11
Verde, L., Bernal, J. L., Heavens, A. F., & Jimenez, R. 2017, MNRAS, 467, 731
Verde, L., Treu, T., & Riess, A. G. 2019, Nat. Astron., 3, 891
Wojtak, R., & Agnello, A. 2019, MNRAS, 486, 5046
Wong, K. C., Suyu, S. H., Chen, G. C.-F., et al. 2019, MNRAS, 498, 1420
Xu, D., Sluse, D., Schneider, P., et al. 2016, MNRAS, 456, 739
```